

# Polluted White Dwarfs Reveal Exotic Mantle Rock Types on Exoplanets in our Solar Neighborhood

Keith D. Putirka<sup>1</sup>, Siyi Xu<sup>2</sup> (许偲艺)

<sup>1</sup> Corresponding Author; Department of Earth and Environmental Sciences, California State University, Fresno, 2576 E. San Ramon Ave, MS/ST 24, 93740, kputirka@csufresno.edu

<sup>2</sup> Gemini Observatory/NSF's NOIR Lab, #314, 670 N. A'ohoku Place, Hilo, Hawaii, 96720, siyi.xu@noirlab.edu

## Abstract

**Prior studies have hypothesized that some polluted white dwarfs record continent-like granitic crust—which is abundant on Earth and perhaps uniquely indicative of plate tectonics. But these inferences derive from only a few elements, none of which define rock type. We thus present the first estimates of rock types on exoplanets that once orbited polluted white dwarfs—stars whose atmospheric compositions record the infall of formerly orbiting planetary objects—examining cases where Mg, Si, Ca and Fe are measured with precision. We find no evidence for continental crust, or other crust types, even after correcting for core formation. However, the silicate mantles of such exoplanets are discernable: one case is Earth like, but most are exotic in composition and mineralogy. Because these exoplanets exceed the compositional spread of >4,000 nearby main sequence stars, their unique silicate compositions are unlikely to reflect variations in parent star compositions. Instead, polluted white dwarfs reveal greater planetary variety in our solar**

**neighborhood than currently appreciated, with consequently unique planetary accretion and differentiation paths that have no direct counterparts in our Solar System. These require new rock classification schemes, for quartz + orthopyroxene and periclase + olivine assemblages, which are proposed here.**

## **1. Introduction**

White dwarfs have received much attention among exoplanet enthusiasts, as more than a quarter accrete rocky material into their photospheres.<sup>1-2</sup> These so-called “polluted white dwarfs” (PWDs) act as “cosmic mass spectrometers”<sup>3</sup> that provide near-direct analyses of exoplanet compositions. White dwarfs are stars that have left the main sequence, having used up all their fuel; the stars first expand to form red giants, and then contract, to a size that is about that of Earth.<sup>4</sup> At this point, planets orbiting these stars may cross the stellar Roche limit and disintegrate, with the resulting debris falling into the stellar atmospheres.<sup>3-4</sup> Most white dwarfs that have cooled below 25,000 K have atmospheres that consist of pure H or He, as heavier elements sink rapidly to stellar cores at such temperatures.<sup>3-4</sup> When accretion of planetary debris occurs, though, elements heavier than He are detected, giving us our most direct view of exoplanet compositions.<sup>3-4</sup> The pollution sources may consist of entire planets, or the broken bits of planets like our asteroid belt<sup>3-4</sup>. But dynamic modeling<sup>5</sup> indicates that metallic cores might be more resistant to tidal forces, so silicate materials (mantle + crust) might be concentrated in pollution sources—which can magnify our view of mantle and crust compositions.

Early studies of PWDs indicate that pollution sources are quite likely dominated by rocky objects, much like our inner planets<sup>4,6-9</sup>. Astronomers often use the term “Earth-like” for such objects, to distinguish these from gas giants. But as we’ll show, PWDs allow for added precision: Mercury, Earth, Moon, and Mars are all “Earth-like” in astronomical terms, but vastly different geologically. We thus

reserve the term “Earth-like” for planets that are more similar to Earth than they are to Mars, Mercury or the Moon, etc., and recommend modifiers such as “Mars-like” or “Mercury-like”, etc., as occasion demands.

Regarding such precision, recent studies assert that continental crust exists on a number of PWDs.<sup>10-12</sup> In one study<sup>11</sup>, granitic crust is identified on 27 of 29 PWDs, with granitic mass fractions ranging to 75%. If valid, these would be spectacular finds, as continental crust is a defining characteristic of Earth. Such discoveries are thought by some to provide our only means of identifying exoplanetary plate tectonics, or global water cycles, as continental crust seems necessarily linked to these.<sup>13-14</sup> However, identifications of continental crust are based only on nominally high abundances of Ca and Al<sup>10-11</sup>, or ratios of these with Li or other alkali metals<sup>12</sup>, usually plotted on a log scale. But none of these elements define rock type, and elevated Li/Ca, may be more reflective of galactic-scale chemical evolution than rock compositions.<sup>15</sup> Moreover, none of these studies account for Si, let alone simultaneously examine the sum: Si + Mg + Fe + Ca, which account for >90% of anhydrous cations on nearly all rocky bodies<sup>16-17</sup>. The inclusion of Si is especially critical as it is a hallmark of continental crust, where SiO<sub>2</sub> contents average 60 wt. % and range to >75%<sup>18</sup>. Our data include thirteen PWDs where high granitic crust fractions (30–75%) have been proposed,<sup>11</sup> where we identify rock types and test claims of exoplanetary crust compositions.

Here we thus examine 23 PWDs where Ca, Si, Mg and Fe are measured with precision (see Methods). Because PWDs might reflect assimilation of entire planets (mantle + crust + core), we compare their bulk compositions to the bulk compositions of the inner planets of our Solar System, taking estimates of their silicate compositions<sup>19-27</sup> and adding back their metallic cores<sup>28</sup>. Because pollution might be dominated by silicate fractions<sup>5</sup>, we also calculate bulk silicate planet compositions (BSP) that account for the removal of Earth-like core fractions<sup>17</sup> from the bulk compositions, and we compare these (as well as bulk PWDs)

to meteorites<sup>29</sup>, and rocks from Mars<sup>30</sup>, Earth<sup>31</sup> and Moon<sup>32</sup>, as well as the putative silicate fractions of exoplanets calculated from main sequence star compositions in our galactic neighborhood<sup>16-17</sup>.

## Results

We find that our 23 PWDs exhibit compositional ranges that exceed that of the inner planets and the more than 4,000 rocky exoplanet compositions inferred from main sequence stars (Figs. 1a–b). Meteorites capture much of the absolute compositional range of PWDs and a few fall close to chondrites or stony irons (Fig. 1c). However, with their higher Si contents, achondrites<sup>29</sup> and crustal rocks from Mars<sup>30</sup>, Earth<sup>31</sup>, and Moon<sup>32</sup>, all provide poor matches for PWD bulk compositions. Some bulk PWDs overlap in both Mg and Si with a subclass of achondrites, called “urelites” (whose origin and parent body are unknown; Fig. 1c), but urelites have much lower Ca<sup>29</sup> than PWDs. High-Ca PWDs, though, overlap with respect to all four elements with a small subset of continental flood basalts<sup>30</sup> (Fig. 1d).

The high Fe in PWDs (Fig. 1b) indicates that some PWDs could be assimilating not just silicates but also metal, possibly from differentiated cores. Silica contents are increased if we consider Fe subtraction after core formation and so we calculate “bulk silicate planet” (BSP = mantle + crust) compositions for PWDs (Fig. 2), assuming Earth-like partitioning of Fe between silicate and metal reservoirs (where the fraction of Fe in the mantle relative to the bulk planet, noted as  $\alpha_{\text{Fe}}$ , is 0.27)<sup>16</sup>, and compare these to the bulk silicate compositions of Mercury<sup>19</sup>, Earth<sup>21</sup> and Mars<sup>25-26</sup>, as well as to martian<sup>30</sup>, terrestrial<sup>31</sup> and lunar<sup>32</sup> crustal rock compositions (Fig. 2). There is no unique answer to the amount of metallic Fe sequestered into a core, so the precise calculated Fe contents in our BSPs are of little consequence. But even with the ensuing increases in Si, Mg and Ca, PWDs have SiO<sub>2</sub> that is too low and MgO that is too high for any to represent crustal rock types at any significant fraction (Fig. 2). New PWD models show that Mg is often under-estimated, particularly around cool PWDs.<sup>33-34</sup> However, ultramafic

mantle rocks from Earth, such as peridotites<sup>21</sup> and pyroxenites<sup>31</sup>, are characterized by low SiO<sub>2</sub> and high MgO and can explain all but those PWDs that simultaneously range to the lowest SiO<sub>2</sub> and highest MgO contents.

## Discussion

Our results verify that PWDs record the accretion of rocky exoplanets, but they also show that those exoplanets associated with PWDs have compositions that are exotic to our Solar System—sufficiently so to require new rock classification schemes to describe their mineral assemblages (Figure 3; Table 1). However, unlike prior studies<sup>11</sup> we find no evidence of continental crust, or sure signs of any high-fraction crustal materials. Some high-Ca PWDs are not inconsistent with their pollution sources being similar to certain Ca-rich Martian meteorites, or rare Ca-rich volcanic rocks erupted in continental flood basalt provinces on Earth (Table 1). However, these same PWDs (e.g., WD1041+092, which has the highest Ca in our dataset; Fig. 1b) also have high MgO and low SiO<sub>2</sub> (Fig. 1d)—hallmarks of mantle rock types, such as peridotite and pyroxenite. We thus conclude that PWDs record mantle, not crust compositions. This is perhaps not a surprise given that ultramafic mantle rocks are precisely the class of materials we would expect to dominate the silicate fractions of rocky exoplanets: the lunar crust is no more than 10% of the Moon's total mass, while on Earth, the oceanic and continental crusts combine to comprise < 0.5% of Earth's total mass and  $\approx 0.7\%$  of its silicate fraction<sup>35</sup>

We are not the first to raise concerns about elevated Ca. Astronomers tend to focus on ratios of Ca to other elements, and hypothesize that high Ca/Mg in some PWDs could reflect preferential sublimation of Mg<sup>7</sup>, or that high Ca/Fe involves the loss of Fe during planetary heating, as planets form or when parent stars undergo a red giant phase<sup>36-37</sup>. Such cases would obviate the need to compare high-Ca PWDs to continental crust or high-Ca mafic rocks from Earth and Mars. In any case, their high Mg and low Si

shows the overwhelming likelihood that PWDs record planetary mantles, not crusts. Perhaps most intriguing is that just as the bulk inner planets of our Solar System do not cluster about the Sun (Fig. 1), neither do PWDs precisely mimic the compositions of main sequence stars (Figs. 1–2). Studies of Ca/Fe<sup>36</sup> and Na<sup>37-38</sup> in PWDs similarly reveal a wide variety of parent bodies that pollute PWDs, apparently over a considerable range of orbital radii<sup>37</sup>. All these observations show that accretion and planetary differentiation combine to create a wider array of objects than obtained if planets are merely “chondritic” or solar/stellar in bulk composition.

To evaluate this geologic variety we transform PWD compositions into a so-called “normative” or “standard” mineralogy (see Appendix for details), which approximates equilibration at upper mantle conditions on an Earth-sized planet, of ca. 2.0 GPa and 1350°C<sup>17</sup>. A standard mineralogy facilitates interplanetary comparisons absent various model-dependencies and assumptions, such as water contents, thermal evolution, and pressure-density relationships, which are all unknown but greatly affect mineralogy. Mineral abundances are first plotted into the classic ultramafic rock ternary diagram<sup>39</sup> (Fig. 3a) of olivine (Mg,Fe)<sub>2</sub>SiO<sub>4</sub> + orthopyroxene (Mg,Fe)<sub>2</sub>Si<sub>2</sub>O<sub>6</sub> + clinopyroxene Ca(Mg,Fe)Si<sub>2</sub>O<sub>6</sub>; these minerals represent >90% of Earth’s mantle and are the basis of rocks called “peridotite” and “pyroxenite”. Peridotite has >40% olivine, and is the rock type that is expected to also dominate the mantles Moon, Mars, and Mercury (Fig. 3a). Figure 3a thus provides a test of whether PWD materials can be described using the same kinds of rock types that dominate the inner planets of our Solar System. Those PWDs that fall outside such a ternary diagram (Fig. 3a) do so because one or more minerals that form the apices of the ternary are calculated to have negative abundances. In such cases, the PWDs are then recast using new sets of minerals, which leads to the two new ternary classification diagrams (Figs. 3b–c), which can describe PWDs as positive sets of mineral components. Of our 23 PWDs, eleven fall within or adjacent to the ultramafic rock ternary (Fig. 3a; white diamonds), which also describes the mineralogy of the mantles

of Mercury, Earth, Moon and Mars. The remaining PWDs fall well outside this ternary and are exotic to our Solar System in that they lack either olivine or orthopyroxene (both of which dominate the mantles of the inner planets; Fig. 3a). These exotic PWDs either lack olivine and are saturated in quartz (Fig. 3b) or they lack orthopyroxene and are saturated in periclase (Fig. 3c); note that both periclase and quartz are rare to absent from the upper mantles of the inner planets of our Solar System. We thus propose a new naming convention to describe such mantle rock types: “quartz pyroxenites” have >10% each of orthopyroxene, clinopyroxene, and quartz; “quartz orthopyroxenites” have >10 % orthopyroxene and quartz, and < 10% clinopyroxene; “periclase dunites” have >10% each of periclase and olivine, and <10% clinopyroxene; “periclase wehrlites” contain >10% each of periclase, olivine and clinopyroxene; “periclase clinopyroxenites” have <10% olivine and >10% each of periclase and clinopyroxene (Table 1). Note that despite elevated SiO<sub>2</sub>, none of the five PWDs in Fig. 3c (white diamonds) would qualify as continental crust as they are enriched in orthopyroxene (Fig. 3b) due to their high MgO. If new models of low-temperature PWDs are valid<sup>33-34</sup>, then NLTT 43806 might also fall into Fig. 3c. It is perhaps worth emphasizing that while thermodynamic models likely lead to insights regarding the geology of some exoplanets<sup>40-41</sup>, no current thermodynamic models can predict crust thickness, plate tectonics, or lower mantle mineralogy for the PWDs of Figs. 3b–c, or perhaps even most in Fig. 3a, as partial melting experiments on the relevant compositions have yet to be performed. In addition, while PWDs might record single planets that have been destroyed and assimilated piecemeal<sup>42</sup>, the pollution sources might also represent former asteroid belts<sup>5,9</sup>, in which case the individual objects of these belts would necessarily be more mineralogically extreme. If current petrologic models<sup>43</sup> may be extrapolated, though, PWDs with quartz-rich mantles (Fig. 3b) might create thicker crusts, while the periclase-saturated mantles (Fig. 3c) could plausibly yield, on a wet planet like Earth, crusts made of serpentinite, which may greatly affect the

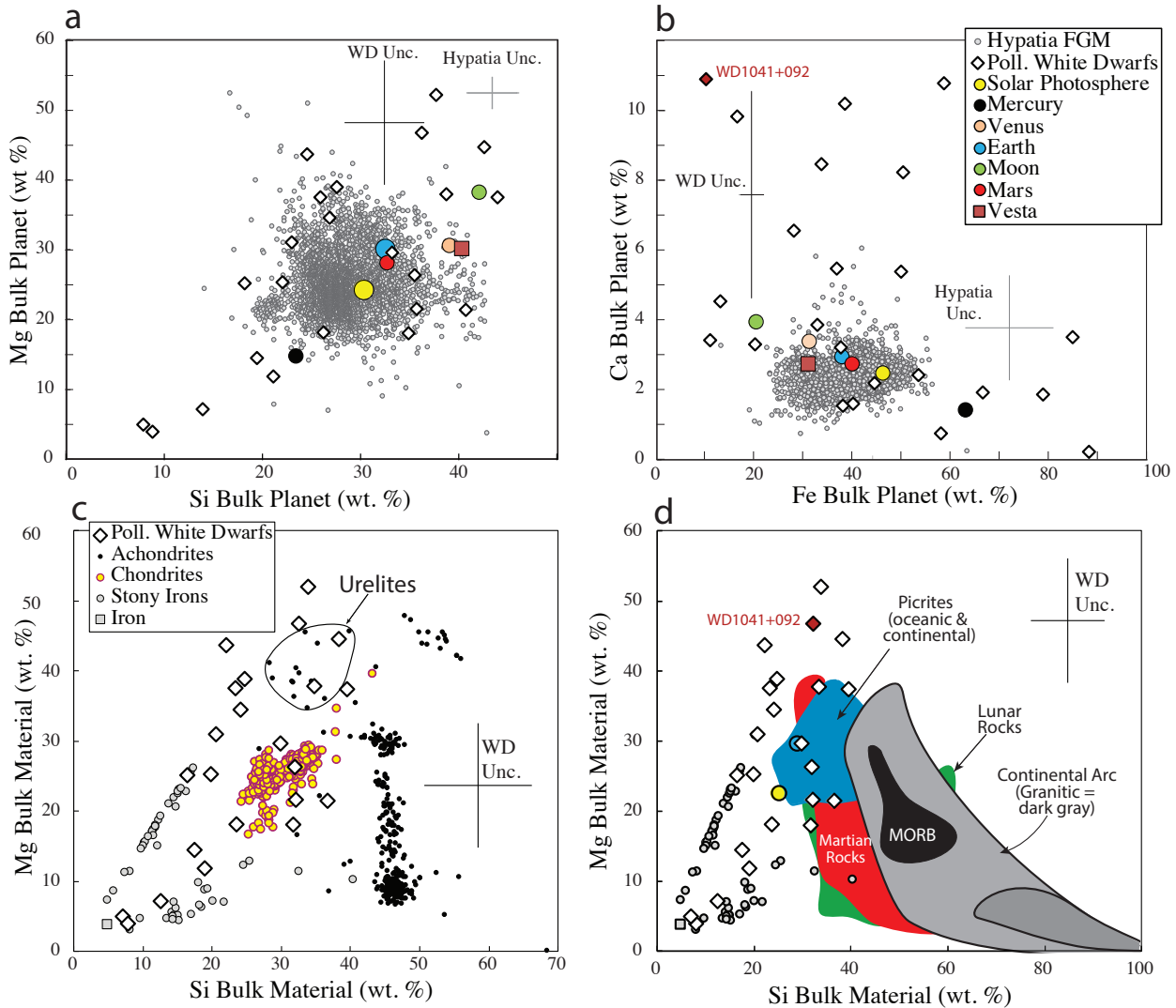
kinds of life that might evolve on the resulting soils.<sup>44</sup> These mineralogical contrasts should also control plate tectonics<sup>45</sup>, although the requisite experiments on rock strength have yet to be carried out.

An interesting result is that, compared to exoplanets inferred to orbit FGKM stars (Fig. 3a), a larger fraction of PWDs fall outside the classic ultramafic rock ternary diagram, and so require our new classification scheme to describe their mantle rock types. This might be an accident, related to our much smaller sampling of PWDs. Another possibility is that FGKM star compositions provide more a view of mean planet composition, and less about absolute lithologic variety in any stellar system. Finally, we cannot rule out the possibility that some PWDs are similar to Earth with respect to crust composition and mineralogy. High K contents identified in LHS 2534<sup>12</sup> are perhaps especially noteworthy, since K is strongly enriched in continental crust. But minor elements, such as K, as well as Li, and Na, do not define rock type and all these elements are fluid mobile and can be enriched in almost any rock type. For example, if high-K PWDs have both high Mg and low Si, they could represent hydrated upper mantle on a water-rich planet, with little direct relevance to crustal compositions. To have a chance at reliable detections of crust compositions (e.g., PWDs with high Si *and* K combined with low Mg), or plate tectonics via our detections of crust compositions<sup>45-46</sup>, we need comprehensive analyses of white dwarfs that include all of what geologists call the “major elements” (Mg, Al, Si, Ca, and Fe) as well as minor elements (Na, K, and Ti) and trace elements that are both highly siderophile (e.g., Ni) and highly lithophile (e.g., U, Ba). Given that Si and Fe vary with galactic radius by orders of magnitude<sup>47</sup>, pursuit of these analyses may well show (if corrections can be made for stellar drift within the galaxy) that some parts of the galaxy are more disposed to forming Earth-like planets than others. Exoplanet studies also force us to face still unresolved questions of why Earth is so utterly different from its immediate planetary neighbors, and whether such contrasts are typical or inevitable<sup>48</sup>.



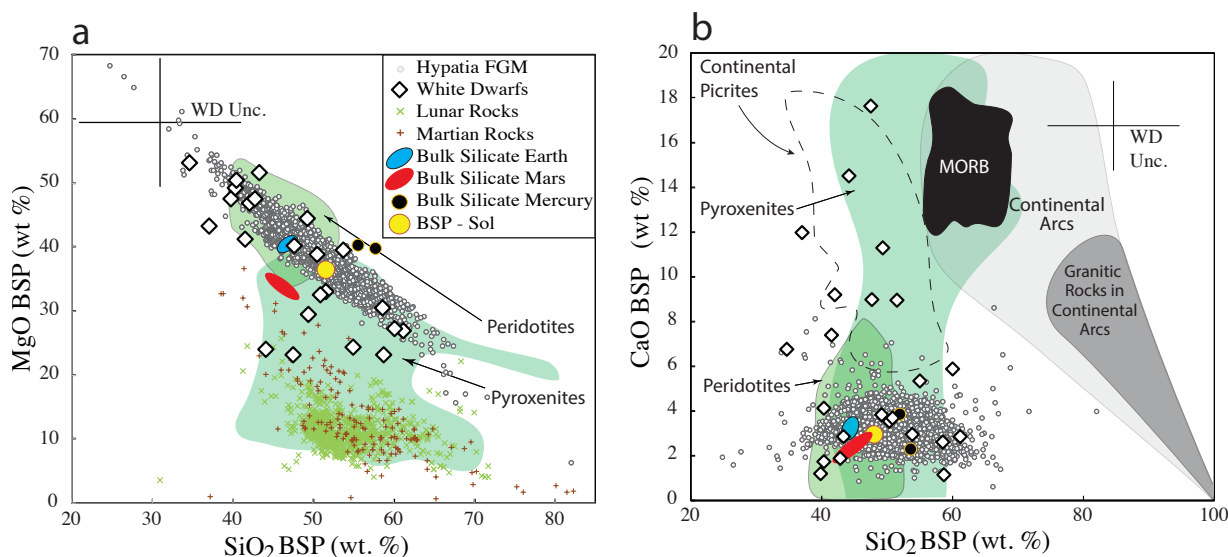
## Figure Captions

Figure 1



**Figure 1.** Bulk compositions of polluted white dwarfs (PWDs) are compared to the bulk planets Earth<sup>21</sup>, Moon<sup>23</sup> and Mars<sup>26</sup> and FGKM stars of the Hypatia Catalog<sup>17</sup> (a–b), and various meteorite types<sup>19</sup> (c), as well as rocks from Earth<sup>31</sup>, Moon<sup>32</sup> and Mars<sup>30</sup>, and iron and stony iron meteorites<sup>19</sup> (d). (c) also shows the field for the subclass of achondrites known as urelites, which have an unknown parentage. Mg + Si + Ca + Fe are normalized to equal 100%. Vertical and horizontal lines labelled “WD Unc.” show the propagated average uncertainties of PWD compositions. (a–b) show that PWDs exhibit a much wider range of compositions than that found among FGKM stars. (c–d) show that PWDs overlap only imperfectly with meteorites from our Solar System, and almost not at all with rocks from Earth, Mars or Moon. WD1041+092 has the highest Ca among our PWDs, but as can be seen in (d), it cannot be a candidate for continental crust as it is far removed from granitic rocks that characterize such crust types. MORB = Mid-Ocean Ridge Basalt.

## Figure 2



**Figure 2.** Bulk silicate planet (BSP) compositions of polluted white dwarfs (PWDs) are compared to bulk silicate compositions of the inner planets<sup>20-22,24-27</sup> and the BSPs inferred from Hypatia stars<sup>17</sup>, as well as (a) mantle rocks from Earth<sup>21</sup> (peridotites and pyroxenites), and (b) crustal rocks from Earth<sup>31</sup>, Moon<sup>32</sup> and Mars. MgO + SiO<sub>2</sub> + CaO + FeO are normalized to 100%. BSPs are PWDs when metallic cores are removed from the bulk PWDs of Figure 1, to allow comparison to silicate compositions of the inner planets. “WD Unc.” indicates the propagated average uncertainty of PWD compositions. (b) shows that Earth’s continental rocks are a poor match for PWD silicate fractions. (a) and (b) show that rocks from Earth’s mantle are a good match for PWDs. But only one PWD matches bulk silicate Earth; most PWDs match rock types that are not dominant on any inner planet. Sol = Solar; MORB = Mid-Ocean Ridge Basalt.

### Figure 3

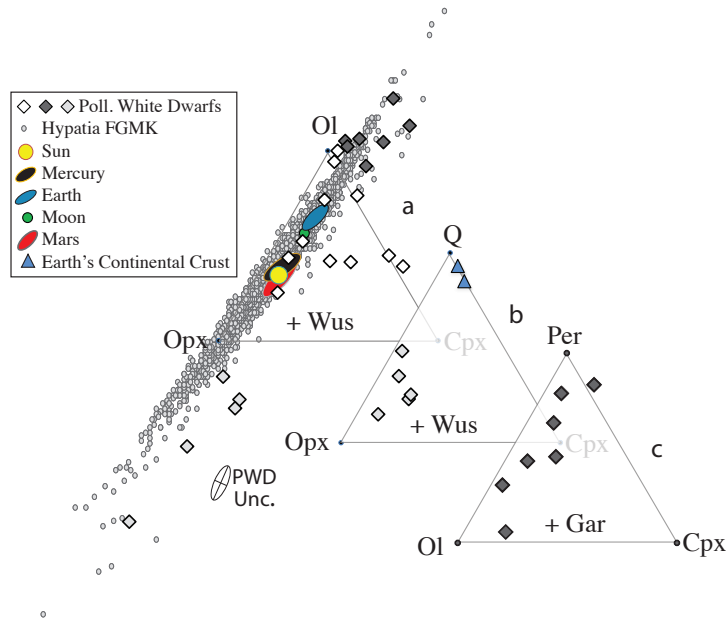


**Figure 3.** Bulk Silicate Planets (Mg + Si + Ca + Fe) of PWDs are recast as mineral components and plotted in (a) the classic ternary ultramafic rock classification<sup>39</sup>, and two new ternary diagrams, (b) and (c), that can describe PWDs as a set of positive mineral components. “PWD Unc.” indicates the propagated average uncertainty in PWD compositions. These ternaries show the relative proportions of the minerals olivine (Ol;  $(\text{Mg,Fe})_2\text{SiO}_4$ ), orthopyroxene (Opx;  $(\text{Mg,Fe})_2\text{Si}_2\text{O}_6$ ), clinopyroxene (Cpx;  $\text{Ca}(\text{Mg,Fe})\text{Si}_2\text{O}_6$ ), periclase (Per; MgO), and quartz (Q;  $\text{SiO}_2$ ). The symbols “+ Wus” and “+ Gar” indicate that all rocks within a given ternary respectively contain wüstite (Wus; FeO) or pyrope garnet (Gar;  $\text{Mg}_3\text{Al}_2\text{Si}_3\text{O}_{12}$ ). Points falling outside a ternary contain a negative amount of one or more indicated minerals and must be recast using a new set of minerals to obtain positive proportions. Mantle compositions of Earth, Moon Mars, and Mercury fall within (a), as do BSPs calculated using FGK star compositions. Many PWDs fall outside of (a), but can be described as positive fractions of either (b) Q + Opx + Cpx, or (c) Per + Ol + Cpx (c). Even in (a), only a few PWDs are mineralogically similar to the inner planets or exoplanets derived from FGK stars. In (b), Q-bearing PWD mantles have too much Opx (too much MgO) to represent continental crust, which plots at much higher Q contents. Suggested rock names for the new classification schemes in (b) and (c) are given in Table 1.

### Acknowledgments

Putirka was supported by NSF grant #1921182. Xu was partly supported by the international Gemini Observatory, a program of NSF’s NOIRLab, which is managed by the Association of Universities for Research in Astronomy (AURA) under a cooperative agreement with the National Science Foundation, on behalf of the Gemini partnership of Argentina, Brazil, Canada, Chile, the Republic of Korea, and the

United States of America. Putirka thanks John Rarick for inspiring this research path. We thank Editor, Sebastian Müller, for his thoughtful handling of our paper, and three anonymous reviewers for their very careful reading of our manuscript and their helpful comments that were much appreciated and greatly improved the final draft.

**Supplementary Information** is available for this paper

**Correspondence** and requests for materials should be addressed to Keith Putirka

**Reprints** and permissions information is available at [www.nature.com/reprints](http://www.nature.com/reprints)

## Methods

We focus on 23 polluted white dwarfs that are located within 200 pc of the Sun, where Mg, Si, Ca and Fe are detected and uncertainties are reported (Supplementary Table A1). Our tests involve high-Ca PWD of prior studies<sup>9-11</sup>, ten of which are reported to have continental crust fractions,  $F_{crust}$ , of 30–75%<sup>11</sup> (Table A3). A larger number of elements could be considered, but only at great sacrifice to the total number of PWDs examined (n=23). Table A1(Supplement) reports star compositions and properties, and published sources. Polluted white dwarfs are compared to star compositions from the Hypatia Catalog<sup>16</sup> which provides compositions of >9,000 main sequence (or FGKM-type) stars that fall within 150 pc of the Sun, and where compositions are known with precision. We take a subset of 4,200 of these where multiple rock-forming elements are reported<sup>17</sup>. All cation sums for all compositions are renormalized to: Mg + Si + Ca + Fe = 100%, or as oxides: MgO + SiO<sub>2</sub> + CaO + FeO = 100% (for the purposes of comparing Fe in oxidized silicate materials, all Fe is expressed as total FeO, or FeOt). Bulk silicate planet compositions are projected as standard upper mantle mineral components, as employed for a prior study of exoplanets inferred from Hypatia Star compositions.<sup>17</sup>

## Data Availability

All data used for this study are published in the accompanying Extended Data tables, which are also available from the lead author upon request.

## Authorship Contributions

The authors, Keith D. Putirka, and Siyi Xu (许偲艺), contributed equally to this work.

## Competing Interests

The authors declare no competing interests

## References Cited

1. Zuckerman, B., Melis, C., Klein, B., Koester, D., Jura, M. Ancient planetary systems are orbiting a large fraction of white dwarf stars. *Astrophys. J.* **722**, 725-736 (2010).

2. Koester, D., Gänsicke, B.T., Farihi, J. The frequency of planetary debris around young white dwarfs. *Astron. Astrophys.* **566**, A34 (2014).
3. Xu, S., Bonsor, A. Exo-geology: insights from dead stars. *Elements* (accepted, no DOI available) (2021).
4. Jura, M., Young, E.D. Extrasolar cosmochemistry. *Ann. Rev. Earth and Planet. Sci.* **42**, 45-67 (2014).
5. Veras, D., Heng, K. The lifetimes of planetary debris discs around white dwarfs. *MNRAS* **496**, 2292-2308 (2020).
6. Jura, M. Pollution of single white dwarfs by accretion of many small asteroids. *The Astron. J.* **135**, 1785-1792 (2008).
7. Xu, S. et al. Compositions of planetary debris around dusty white dwarfs. *Astron. J.* **158**, <https://doi.org/10.3847/1538-3881/ab4cee> (2019).
8. Doyle, A.E., Young, E.D., Klein, B., Zuckerman, B., Schlichting, H.E. Oxygen fugacities of extrasolar rocks: evidence for an Earth-like geochemistry of exoplanets. *Science* **366**, 356-359 (2019).
9. Gänsicke, B.T. et al. The chemical diversity of exo-terrestrial planetary debris around white dwarfs. *Month. Not. Royal Astron. Soc.* **424**, 333-347 (2012).
10. Zuckerman, B. et al. An aluminum/calcium-rich, iron-poor, white dwarf star: evidence for an extrasolar planetary lithosphere. *Astrophys. J.* **739**, 101 (2011).
11. Hollands, M.A., Gänsicke, B.T., Koester, D. Cool DZ white dwarfs II: compositions and evolution of old remnant planetary systems. *MNRAS* **477**, 93-111(2018).

12. Hollands, M.A., Tremblay, P-E., Gänsicke, B.T., Koester, D., Gentile-Fusillo, N.P. Alkali metals in white dwarf atmospheres as tracers of ancient planetary crusts. *Nat. Astron.* doi.org/10.1038/s41550-020-01296-7 (2021).
13. Campbell, I.H., Taylor, S.R. No water, no granites – no oceans, no continents. *Geophys. Res. Lett.* **10**, 1061-1064(1983).
14. Tatsumi, Y., Sato, T., Kodaira, S. Evolution of the Earth as an andesite planet: water, plate tectonics, and delamination of anti-continent. *Earth, Planet. Space* **67**, 91, DOI 10.1186/s40623-015-0267-2 (2015).
15. Kaiser, B.C. et al. Lithium pollution of a white dwarf records the accretion of an extrasolar planetesimal. *Science*, **371**, 168-172 (2021).
16. Hinkel, N.R., Timmes, F.X., Young, P.A., Pagano, M.D., Turnbull, M.C. Stellar abundances in the solar neighborhood: the Hypatia Catalog. *Astron. J.* **148**, 54 (33 pp) (2014).
17. Putirka, K., Rarick, J.C. The composition and mineralogy of rocky exoplanets: a survey of >4,000 stars from the Hypatia Catalog. *Am. Mineral.* **104**, 817-829 (2019).
18. Rudnick, R.L., Gao, S. Composition of the continental crust. *Treat. Geochem.* **3**, 2<sup>nd</sup> ed. 1-51 (2014).
19. Nittler, L.R., Chabot, N.L., Grove, T.L., Peplowski, P.N. The Chemical Composition of Mercury. Mercury: The View after MESSENGER Ch 2. (Cambridge: Cambridge University Press, Cambridge, 2018).
20. Morgan, J.W., Anders, E. Chemical composition of Earth, Venus, and Mercury. *Proc. Nat. Acad. Sci. U.S.A.* **77**, 6973-6977 (1980).
21. McDonough, W.F., Sun, S.-s. The composition of the Earth. *Chem. Geol.* **120**, 223-253 (1995).
22. Longhi, J. Petrogenesis of picritic mare magmas: constraints on the extent of lunar differentiation. *Geochim. Cosmochim. Acta* **70**, 5919-5934 (2006).

23. Jones, J.H., Delano, J.W. A three-component model for the bulk composition of the Moon. *Geochim. Cosmochim. Acta* **53**, 513-527 (1989).
24. Khan, A., Pommier, A., Neumann, G.A., Mosegaard, K. The lunar moho and the internal structure of the Moon: a geophysical perspective. *Tectonophys.* **609**, 331-352 (2013).
25. Khan, A., Connolly, J.A.D. Constraining the composition and thermal state of Mars from inversion of geophysical data. *J. Geophys. Res. Planet.* **113**, E07003 (2008).
26. Yoshizaki, T., McDonough, W.F. The composition of Mars. *Geochim. Cosmochim. Acta* **273**, 137-162 (2020).
27. Steenstra, E.S., Knibbe, J.S., Rai, N., van Westrenen, W. Constraints on core formation in Vesta from metal-silicate partitioning of siderophile elements. *Geochim. Cosmochim. Acta* **177**, 48-61 (2016).
28. Szurgot, M. Core mass fraction and mean atomic weight of terrestrial planets, Moon, and protoplanet Vesta. *Compar. Tect. Geodyn.* **5001**.pdf (2015).
29. Nittler, L.R., et al. Bulk element compositions of meteorites: a guide for interpreting remote-sensing geochemical measurements of planets and asteroids. *Ant. Met. Res.* **17**, 233-253 (2004).
30. Udry, A. et al. What Martian meteorites reveal about the interior and surface of Mars. *JGR Planet.* <https://doi.org/10.1029/2020JE006523> (2020).
31. Sarbas, B. The GEOROC database as part of a growing geoinformatics network. *Geoinformatics* (2008)
32. Meyer, C. Lunar Sample Compendium. NASA Sample collections, <https://curator.jsc.nasa.gov/lunar/lsc/> (2012).
33. Blouin, S. Magnesium abundances in cool metal-polluted white dwarfs. *MNRAS* **496**, 1881-1980 (2020).

34. Turner, S.G.D., Wyatt, M.C. Modelling the distributions of white dwarf atmospheric pollution: a low Mg abundance for accreted planetesimals? *MNRAS* **491**, 4672-4689 (2020).
35. Lodders, K., Fegley, B. Jr. The planetary scientists companion. Oxford University Press, NY, NY, 371 pp., ISBN 0-19-1511694-1 (1998).
36. Bonsor, A. et al. Are exoplanets differentiated? *MNRAS* **492**, 2683-2697 (2020).
37. Harrison, J.H.D. et al. Bayesian constraints on the origin and geology of exoplanetary materials using a population of externally polluted white dwarfs. *MNRAS* **504**, 2853-2867 (2021).
38. Swan, A. et al. Interpretation and diversity of exoplanetary material orbiting white dwarfs. *MNRAS* **490**, 202-218 (2019)
39. Le Bas, M.J., Streckeisen, A.L. The IUGS systematics of igneous rocks. *J. Geol. Soc. Lond.* **148**, 825-833 (1991).
40. Hinkel, N.R., Unterborn, C.T. The star-planet connection I: using stellar composition to observationally constrain planetary mineralogy for the ten closest stars. *Astrophys. J* **853**, 83 (2018).
41. Unterborn, C.T. et al. Stellar chemical clues as to the rarity of exoplanetary tectonics. Preprint at: *arXiv:1706.10282v2 [astro-ph.EP]* (2017).
42. Harrison, J.D., Bonsor, A., Madhusudhan, N. Polluted white dwarfs: constraints on the origin and geology of exoplanetary material. *MNRAS* **479**, 3814-3841 (2018).
43. Lambart, S., Baker, M.B., Stolper, E.M. The role of pyroxenite in basalt genesis: MELT-PX, a melting parameterization for mantle pyroxenites between 0.9 and 5 GPa. *J. Geophys. Res.*, doi:10.1002/2015JB012762 (2016).
44. McGahn, D.G., Southard, R.J., Claassen, V.P. Plant available calcium varies widely in soils on serpentinite landscapes. *SSSAJ*, 73, 2087-2095 (2009).



45. Weller, M.B., Lenardic, A. On the evolution of terrestrial planets: bi-stability, stochastic effects, and the non-uniqueness of tectonic states. *Geosci. Front.* **9**, 91-201 (2018).
46. Jura, M., Klein, B., Xu, S., Young, E.D. A pilot search for evidence of extrasolar earth-analog plate tectonics. *Astrophys. J. Lett.* **791**:L29 (2014).
47. Luck, R.E., Lambert, D.L. The distribution of the elements in the galactic disk. III. A reconsideration of cepheids from  $l = 30^\circ$  to  $250^\circ$ . *Astron. J.* **142**, 136 (2011).
48. Hazen, R.M., Grew, E.S., Downs, R.T., Golden, J., Hystad, G. Mineral ecology; chance and necessity in the mineral diversity of terrestrial planets. *Can. Mineral.* **53**, 295–324 (2015).

Table 1. Mantle Mineral Modes and Rock Types, Calculated From Bulk Silicate Planet Compositions.

| White Dwarf          | Olivine<br>(Mg,Fe) <sub>2</sub> SiO <sub>4</sub> | Clinopyroxene<br>Ca(Mg,Fe)Si <sub>2</sub> O <sub>6</sub> | Orthopyroxene<br>(Mg,Fe) <sub>2</sub> SiO <sub>6</sub> | Quartz<br>SiO <sub>2</sub> | Periclase<br>MgO | Mantle Rock Type <sup>b</sup>    |
|----------------------|--|--|--|----------------------------|------------------|----------------------------------|
| PG0843+517           |  | 3.2  | 48.1   | 48.7                       |                  | <b>Quartz Orthopyroxenite</b>    |
| WD1929+011           | 100.6  | 3.3  | -3.9   |                            |                  | Dunite                           |
| WD1536+520           | 47.0   | 9.4  |  |                            | 43.6             | <b>Periclase Dunite</b>          |
| PG1015+161           |  | 18.2   | 55.8   | 26.0                       |                  | <b>Quartz Pyroxenite</b>         |
| Ton345               |  | 8.8  | 75.6   | 15.6                       |                  | <b>Quartz Orthopyroxenite</b>    |
| WD1041+092           | -3.9   | 20.1   |  |                            | 83.8             | <b>Periclase Clinopyroxenite</b> |
| HE0106-3253          | 45.5   | 54.4   | 0.1  |                            |                  | Wehrlite                         |
| GD61                 | 74.3   | 10.5   | 15.2   |                            |                  | Lherzolite                       |
| GD40                 | 32.5   | 21.6   |  |                            | 45.9             | <b>Periclase Wehrlite</b>        |
| G241-6               | 24.8   | 11.3   |  |                            | 63.8             | <b>Periclase Wehrlite</b>        |
| WD1551+175           | 42.3   | 29.4   | 28.4   |                            |                  | Lherzolite                       |
| WD2207+121           | 52.9   | 11.2   | 35.9   |                            |                  | Lherzolite                       |
| WD1145+017           | 25.7   | 13.5   | 60.8   |                            |                  | Olivine Websterite               |
| WD 1425+540          |  | 8.2  | 56.3   | 35.5                       |                  | <b>Quartz Orthopyroxenite</b>    |
| HS2253+8023          | 75.6   | 18.0   |  |                            | 6.4              | <b>Periclase Wehrlite</b>        |
| WDJ0738+1835         | 94.5   | 4.9  | 0.6  |                            |                  | Dunite                           |
| WDJ1242+5226         | 44.2   | 9.2  | 46.6   |                            |                  | Harzburgite or Aubrite           |
| G29-38               |  | 18.5   | 58.1   | 23.4                       |                  | <b>Quartz Pyroxenite</b>         |
| WD1232+563           | 64.5   | 4.2  |  |                            | 31.2             | <b>Periclase Dunite</b>          |
| PG1225-079           | 41.6   | 38.9   | 19.5   |                            |                  | Lherzolite                       |
| GD362                | 39.6   | 63.8   | -3.5   |                            |                  | Olivine Clinopyroxenite          |
| Ross640              | 13.1   | 7.4  |  |                            | 79.5             | <b>Periclase Dunite</b>          |
| NLTT43806            | 76.6   | 24.6   | -1.2   |                            |                  | Wehrlite                         |
| Sol-BSP <sup>a</sup> | 34.3   | 10.5   | 55.2   |                            |                  | <i>Olivine Websterite</i>        |

(a) Sol-BSP is the mineralogy of a rocky planet that has a Solar bulk composition, with an Earth-like amount of Fe partitioned into a metallic core.<sup>17</sup> (b) Rock names that are not in bold italics are for ultramafic rocks from our Solar System<sup>33</sup>; names in **bold italic** font

---

are new, proposed names guided by Figs. 3b–c: “quartz pyroxenites” have >10% each of orthopyroxene, clinopyroxene, and quartz; “quartz orthopyroxenites” have >10 % orthopyroxene and quartz, and < 10% clinopyroxene; “periclase dunites” have >10% each of periclase and olivine, and <10% clinopyroxene; “periclase wehrlites” contain >10% each of periclase, olivine and clinopyroxene; “periclase clinopyroxenites” have <10% olivine and >10% each of periclase and clinopyroxene.

---

## Supplementary Data & Equations

Polluted white dwarf compositions are typically reported as either  $\log(Z/Y) = \log[n(Z)/n(H)]$  or  $\log(Z/Y) = \log[n(Z)/n(He)]$ , where  $n(Z)$  is the number of atoms of the element of interest,  $Z$ , and in the denominator,  $n(Y)$  is the number of atoms of either H or He, depending upon which dominates a PWD's atmosphere. Since  $Y$  is the same for any given PWD, cation fractions for any given star can be obtained by renormalization irrespective of  $Y$ , so that  $10^{[Mg/Y]} + 10^{[Si/Y]} + 10^{[Ca/Y]} + 10^{[Fe/Y]} = 100\% = Mg + Si + Ca + Fe$ , on the basis of numbers of atoms; multiplication by atomic weights and renormalization provides weight % values. In the Hypatia Catalog, main sequence star compositions are reported as a difference in log concentrations relative to the Sun (always as  $[Z/H]$ ) and thus require a correction using solar elemental abundances (Lodders et al. 2009). Cations of meteorites are often plotted as  $Z/Si$ , but reported values are given as cation or oxide percentages. Error bars for PWDs use reported uncertainties in the literature to derive the standard deviations from 1,000 Monte Carlo simulations (assuming a normal distribution) to arrive at an average uncertainty; median reported uncertainties in the literature (which in units of  $\log(Z/Y)$  are:  $\pm 0.18$  dex Mg;  $\pm 0.15$  dex Si;  $\pm 0.156$  dex Ca;  $\pm 0.12$  dex Fe). Error bars on Hypatia compositions are propagated from the compositional “spread” of Hinkel et al. (2014, 2016); Monte Carlo simulations on analytical uncertainties reported in Hinkel et al. (2014) would yield very much smaller error bars than reported here, but it is not clear that such uncertainties are fully representative of star composition uncertainties (see Hinkel et al. 2014). Uncertainties for Earth and Martian compositions, where shown, represent standard deviations from McDonough and Sun (1995) and Yoshizaki and McDonough (2020), and “high” and “low” values of Khan and Connelly (2008).

### *Calculating Bulk Silicate Planet Compositions*

In addition to comparing bulk materials, we also calculate Bulk Silicate Planet (BSP) compositions for PWDs, using the methods applied to Hypatia stars in Putirka and Rarick (2019) (Table A2). We compare these to silicate compositions from our Solar System. Oxygen is sufficiently abundant in parent FGKM stars (Unterborn and Panero 2017; Putirka and Rarick 2019) and PWDs (Doyle et al. 2019) so that Mg, Si and Ca are almost certainly fully oxidized (to MgO, SiO<sub>2</sub> and CaO) and some fraction of Fe is oxidized to FeO, depending upon a planet's oxygen fugacity ( $fO_2$ ). As a proxy for  $fO_2$ , we apply the approach of Putirka and Rarick (2019) using:  $\alpha_{Fe} = Fe^{BSP}/Fe^{BP}$ , where  $Fe^{BSP}$  is the cation fraction of Fe in the bulk silicate planet (crust + mantle), and  $Fe^{BP}$  is the cation fraction of Fe in the bulk planet (crust + mantle + core). Since total oxygen contents for PWDs are roughly Earth-like (Doyle et al. 2019), although perhaps slightly more oxidized on average, we apply a terrestrial  $\alpha_{Fe} = 0.27$  (see Putirka and Rarick 2019). Finally, we test the algebraic methods of Hollands et al (2018) to calculate crust fractions of PWDs, using a mantle composition from McDonough and Sun (1995), an average crust composition from Rudnick and Gao (2014), an oceanic crust composition from Gale et al. (2013), and a core that contains 7% Si (Wade and Wood 2005) in addition to Fe. Hollands et al. (2018) use matrices to recast reservoir (core, mantle and crust) compositions into the mass fractions of each. In such a method, FeO in a silicate mantle is fixed, so  $fO_2$  will implicitly vary for each PWD (using a fixed value for  $\alpha_{Fe}$  a constant  $fO_2$  is implicit and FeO contents in the mantle will vary; Table A2).

Bulk planetary compositions for the inner planets are computed, using metal core/silicate fractions of Szurgot (2015) and assuming that metal cores are 100 wt. % Fe, except for Earth, where we assume the core has 88 wt. % Fe and 7% Si (e.g., Wade and Wood 2005; Wood et al. 2014). We also compare PWDs to mean continental crust composition from Rudnick and Gao (2014), average mid-ocean ridge basalt from Gale et al. (2013), and to various rock types, including mid-ocean ridge and ocean island basalts, oceanic island arcs and picrites from various tectonic settings, from the GEOROC database

(<http://georoc.mpch-mainz.gwdg.de/georoc/>) and plutonic rocks of all types from the Sierra Nevada, as an example of upper continental crust, from the NAVDAT database (<https://www.navdat.org/>).

N.b.: the apparent positive and negative correlations in Fig. 1 in the main text are artifacts of the constant sum effect, which is amplified by projecting compositions into a four-component space that is dominated by three elements; see Chayes (1960) and Putirka and Rarick (2019). The positive correlation of Mg v Si for the terrestrial planets, for example, disappears ( $R^2 = 0.19$ ) for MgO v. SiO<sub>2</sub> within a 10-oxide system.

### Geochemical Projections

To test Hollands et al.'s (2018) identification and quantification of silicate crust fractions from extrasolar systems, we apply their algebraic approach to calculate crust, mantle and core fractions of the PWDs of Table 1. Their strategy was to use Earth-like compositions (using Ca, Mg and Fe) for the crust, mantle and core as inputs, so that for a three component system, a 3 x 3 matrix can relate bulk PWD compositions to the fractions of crust, mantle and core. Expressing the mass balance using row matrices, we have:

$$\begin{bmatrix} C_{\text{SiO}_2}^{\text{BPWD}} & C_{\text{FeO}}^{\text{BPWD}} & C_{\text{MgO}}^{\text{BPWD}} \end{bmatrix} = \begin{bmatrix} F_{\text{Crust}} & F_{\text{Mantle}} & F_{\text{Core}} \end{bmatrix} \begin{bmatrix} C_{\text{SiO}_2}^{\text{Crust}} & C_{\text{FeO}}^{\text{Crust}} & C_{\text{MgO}}^{\text{Crust}} \\ C_{\text{SiO}_2}^{\text{Mantle}} & C_{\text{FeO}}^{\text{Mantle}} & C_{\text{MgO}}^{\text{Mantle}} \\ C_{\text{SiO}_2}^{\text{Core}} & C_{\text{FeO}}^{\text{Core}} & C_{\text{MgO}}^{\text{Core}} \end{bmatrix} \quad (\text{A1.1})$$

or alternatively, as column matrices (where superscript T represents the transpose of the square matrix):

$$\begin{bmatrix} C_{\text{SiO}_2}^{\text{BPWD}} \\ C_{\text{FeO}}^{\text{BPWD}} \\ C_{\text{MgO}}^{\text{BPWD}} \end{bmatrix} = \begin{bmatrix} C_{\text{SiO}_2}^{\text{Crust}} & C_{\text{FeO}}^{\text{Crust}} & C_{\text{MgO}}^{\text{Crust}} \\ C_{\text{SiO}_2}^{\text{Mantle}} & C_{\text{FeO}}^{\text{Mantle}} & C_{\text{MgO}}^{\text{Mantle}} \\ C_{\text{SiO}_2}^{\text{Core}} & C_{\text{FeO}}^{\text{Core}} & C_{\text{MgO}}^{\text{Core}} \end{bmatrix}^T \times \begin{bmatrix} F_{\text{Crust}} \\ F_{\text{Mantle}} \\ F_{\text{Core}} \end{bmatrix} \quad (\text{A1.2})$$

where  $C_i^j$  is the weight % concentration of oxide (or element)  $i$  in reservoir  $j$ ,  $F_j$  is the mass fraction of reservoir  $j$  and the superscript BPWD is the bulk composition of polluted white dwarfs (keeping in mind that renormalization is required after matrix multiplication). The Hollands et al. (2018) projection is in the system Ca-Mg-Fe, and as an independent, and perhaps more precise test (reported uncertainties on Si are much less than on Ca), we use the system Si-Fe-Mg. For our system, rearrangement of Equation A1 (where the superscript -1 indicates the inverse of a matrix) yields:

$$\begin{bmatrix} F_{\text{Crust}} & F_{\text{Mantle}} & F_{\text{Core}} \end{bmatrix} = \begin{bmatrix} C_{\text{SiO}_2}^{\text{BPWD}} & C_{\text{FeO}}^{\text{BPWD}} & C_{\text{MgO}}^{\text{BPWD}} \end{bmatrix} \times \begin{bmatrix} C_{\text{SiO}_2}^{\text{Crust}} & C_{\text{FeO}}^{\text{Crust}} & C_{\text{MgO}}^{\text{Crust}} \\ C_{\text{SiO}_2}^{\text{Mantle}} & C_{\text{FeO}}^{\text{Mantle}} & C_{\text{MgO}}^{\text{Mantle}} \\ C_{\text{SiO}_2}^{\text{Core}} & C_{\text{FeO}}^{\text{Core}} & C_{\text{MgO}}^{\text{Core}} \end{bmatrix}^{-1} \quad (\text{A2.1})$$

or alternatively, as column matrices (where the superscript T represents the transpose of a matrix):

$$\begin{bmatrix} F_{\text{Crust}} \\ F_{\text{Mantle}} \\ F_{\text{Core}} \end{bmatrix} = \left[ \begin{bmatrix} C_{\text{SiO}_2}^{\text{Crust}} & C_{\text{FeO}}^{\text{Crust}} & C_{\text{MgO}}^{\text{Crust}} \\ C_{\text{SiO}_2}^{\text{Mantle}} & C_{\text{FeO}}^{\text{Mantle}} & C_{\text{MgO}}^{\text{Mantle}} \\ C_{\text{SiO}_2}^{\text{Core}} & C_{\text{FeO}}^{\text{Core}} & C_{\text{MgO}}^{\text{Core}} \end{bmatrix}^T \right]^{-1} \times \begin{bmatrix} C_{\text{SiO}_2}^{\text{BPWD}} \\ C_{\text{FeO}}^{\text{BPWD}} \\ C_{\text{MgO}}^{\text{BPWD}} \end{bmatrix} \quad (\text{A2.2})$$

For Eqn. A1, we use the bulk silicate Earth composition from McDonough and Sun (1995), a metallic core composition that contains 7 wt. % Si and 88 wt. % Fe (Wood et al. 2014) and we calculate Earth's bulk crust composition using the average continental crust of Rudnick and Gao (2014), the average oceanic crust composition of Gale et al. (2013), and crust masses from Petersen and DePaolo (2007), where the continental crust mass is  $2.17 \times 10^{22}$  kg, and the oceanic crust mass is  $5.99 \times 10^{21}$  kg. (Note: estimates of "bulk silicate Earth" are effectively equal to Earth's mantle. The mantle has a mass of ca.  $4.0 \times 10^{24}$  kg, and so the crust is just under 0.7 wt. % of the total mass of the silicate Earth and is inconsequential for the total abundances of the major elements or oxides). After renormalization so that  $\text{SiO}_2 + \text{FeO} + \text{MgO} + \text{CaO} = 100$  for each reservoir, we have:

$$\begin{bmatrix} C_{\text{SiO}_2}^{\text{Crust}} & C_{\text{FeO}}^{\text{Crust}} & C_{\text{MgO}}^{\text{Crust}} \\ C_{\text{SiO}_2}^{\text{Mantle}} & C_{\text{FeO}}^{\text{Mantle}} & C_{\text{MgO}}^{\text{Mantle}} \\ C_{\text{SiO}_2}^{\text{Core}} & C_{\text{FeO}}^{\text{Core}} & C_{\text{MgO}}^{\text{Core}} \end{bmatrix} = \begin{bmatrix} 74.2 & 9.5 & 6.8 \\ 47.7 & 8.5 & 40 \\ 11.6 & 88.4 & 0 \end{bmatrix} \quad (\text{A2.3})$$

Mineral modes (Figure 3 of main text) are calculated similarly, from bulk silicate planet (BSP) compositions (Table A2) expressed as mole fractions ( $X_i^{\text{BSP}}$ , where the subscript  $i$  is an oxide of interest, such as  $\text{SiO}_2$ ,  $\text{MgO}$ ,  $\text{FeO}$  or  $\text{CaO}$ ), and the mole fractions of various mineral phases ( $X_j$ , where  $j$  is the mineral phase in question). This is effectively the method of Thompson (1982). The mineral fractions ( $F_j$ ) of about half of PWDs can be described as positive (or negative but very nearly zero) amounts of olivine (Ol), clinopyroxene (Cpx), orthopyroxene (Opx) and wüstite (Wus); the mass balance expressed as row matrices is:

$$[F_{\text{Ol}} \ F_{\text{Cpx}} \ F_{\text{Opx}} \ F_{\text{Wus}}] = [X_{\text{SiO}_2}^{\text{BSP}} \ X_{\text{FeO}}^{\text{BSP}} \ X_{\text{MgO}}^{\text{BSP}} \ X_{\text{CaO}}^{\text{BSP}}] \times \begin{bmatrix} X_{\text{SiO}_2}^{\text{Ol}} & X_{\text{FeO}}^{\text{Ol}} & X_{\text{MgO}}^{\text{Ol}} & X_{\text{CaO}}^{\text{Ol}} \\ X_{\text{SiO}_2}^{\text{Cpx}} & X_{\text{FeO}}^{\text{Cpx}} & X_{\text{MgO}}^{\text{Cpx}} & X_{\text{CaO}}^{\text{Cpx}} \\ X_{\text{SiO}_2}^{\text{Opx}} & X_{\text{FeO}}^{\text{Opx}} & X_{\text{MgO}}^{\text{Opx}} & X_{\text{CaO}}^{\text{Opx}} \\ X_{\text{SiO}_2}^{\text{Wus}} & X_{\text{FeO}}^{\text{Wus}} & X_{\text{MgO}}^{\text{Wus}} & X_{\text{CaO}}^{\text{Wus}} \end{bmatrix}^{-1} \quad (\text{A3.1})$$

or as column matrices, is:

$$\begin{bmatrix} F_{\text{Ol}} \\ F_{\text{Cpx}} \\ F_{\text{Opx}} \\ F_{\text{Wus}} \end{bmatrix} = \begin{bmatrix} X_{\text{SiO}_2}^{\text{Ol}} & X_{\text{FeO}}^{\text{Ol}} & X_{\text{MgO}}^{\text{Ol}} & X_{\text{CaO}}^{\text{Ol}} \\ X_{\text{SiO}_2}^{\text{Cpx}} & X_{\text{FeO}}^{\text{Cpx}} & X_{\text{MgO}}^{\text{Cpx}} & X_{\text{CaO}}^{\text{Cpx}} \\ X_{\text{SiO}_2}^{\text{Opx}} & X_{\text{FeO}}^{\text{Opx}} & X_{\text{MgO}}^{\text{Opx}} & X_{\text{CaO}}^{\text{Opx}} \\ X_{\text{SiO}_2}^{\text{Wus}} & X_{\text{FeO}}^{\text{Wus}} & X_{\text{MgO}}^{\text{Wus}} & X_{\text{CaO}}^{\text{Wus}} \end{bmatrix}^{\text{T}}^{-1} \times \begin{bmatrix} X_{\text{SiO}_2}^{\text{BSP}} \\ X_{\text{FeO}}^{\text{BSP}} \\ X_{\text{MgO}}^{\text{BSP}} \\ X_{\text{CaO}}^{\text{BSP}} \end{bmatrix} \quad (\text{A3.1})$$

where the superscript -1 represents the inverse of a matrix and the superscript T represents the transpose of a matrix. To describe the mineral compositions in our "standard mineralogy", we use:

$$\begin{bmatrix} X_{\text{SiO}_2}^{\text{Ol}} & X_{\text{FeO}}^{\text{Ol}} & X_{\text{MgO}}^{\text{Ol}} & X_{\text{CaO}}^{\text{Ol}} \\ X_{\text{SiO}_2}^{\text{Cpx}} & X_{\text{FeO}}^{\text{Cpx}} & X_{\text{MgO}}^{\text{Cpx}} & X_{\text{CaO}}^{\text{Cpx}} \\ X_{\text{SiO}_2}^{\text{Opx}} & X_{\text{FeO}}^{\text{Opx}} & X_{\text{MgO}}^{\text{Opx}} & X_{\text{CaO}}^{\text{Opx}} \\ X_{\text{SiO}_2}^{\text{Wus}} & X_{\text{FeO}}^{\text{Wus}} & X_{\text{MgO}}^{\text{Wus}} & X_{\text{CaO}}^{\text{Wus}} \end{bmatrix} = \begin{bmatrix} 1 & 0.2 & 1.8 & 0 \\ 2 & 0.2 & 0.8 & 1 \\ 2 & 0.2 & 1.8 & 0 \\ 0 & 1 & 0 & 0 \end{bmatrix} \quad (\text{A4})$$

Which represents the specific mineral formulas as follows: olivine =  $\text{Mg}_{1.8}\text{Fe}_{0.2}\text{SiO}_4$ ; clinopyroxene =  $\text{CaMg}_{0.8}\text{Fe}_{0.2}\text{Si}_2\text{O}_6$ ; orthopyroxene =  $\text{Mg}_{1.8}\text{Fe}_{0.2}\text{Si}_2\text{O}_6$ ; wüstite =  $\text{FeO}$ , which are typical compositions for mantle equilibrated conditions that are close to 1300°C and 2 GPa, which represents are “standard” of equilibration.

Those PWDs that have large negative amounts of olivine when applying Eqns. A3–A4 can be described as positive combinations of Wus, Cpx, Quartz (Qtz) and Opx, using the equations:

$$\begin{bmatrix} F_{\text{Wus}} \\ F_{\text{Cpx}} \\ F_{\text{Qtz}} \\ F_{\text{Opx}} \end{bmatrix} = \begin{bmatrix} X_{\text{SiO}_2}^{\text{Wus}} & X_{\text{FeO}}^{\text{Wus}} & X_{\text{MgO}}^{\text{Wus}} & X_{\text{CaO}}^{\text{Wus}} \\ X_{\text{SiO}_2}^{\text{Cpx}} & X_{\text{FeO}}^{\text{Cpx}} & X_{\text{MgO}}^{\text{Cpx}} & X_{\text{CaO}}^{\text{Cpx}} \\ X_{\text{SiO}_2}^{\text{Qtz}} & X_{\text{FeO}}^{\text{Qtz}} & X_{\text{MgO}}^{\text{Qtz}} & X_{\text{CaO}}^{\text{Qtz}} \\ X_{\text{SiO}_2}^{\text{Opx}} & X_{\text{FeO}}^{\text{Opx}} & X_{\text{MgO}}^{\text{Opx}} & X_{\text{CaO}}^{\text{Opx}} \end{bmatrix}^{\text{T}-1} \times \begin{bmatrix} X_{\text{SiO}_2}^{\text{BSP}} \\ X_{\text{FeO}}^{\text{BSP}} \\ X_{\text{MgO}}^{\text{BSP}} \\ X_{\text{CaO}}^{\text{BSP}} \end{bmatrix} \quad (\text{A5})$$

using the following matrix:

$$\begin{bmatrix} X_{\text{SiO}_2}^{\text{Wus}} & X_{\text{FeO}}^{\text{Wus}} & X_{\text{MgO}}^{\text{Wus}} & X_{\text{CaO}}^{\text{Wus}} \\ X_{\text{SiO}_2}^{\text{Cpx}} & X_{\text{FeO}}^{\text{Cpx}} & X_{\text{MgO}}^{\text{Cpx}} & X_{\text{CaO}}^{\text{Cpx}} \\ X_{\text{SiO}_2}^{\text{Qtz}} & X_{\text{FeO}}^{\text{Qtz}} & X_{\text{MgO}}^{\text{Qtz}} & X_{\text{CaO}}^{\text{Qtz}} \\ X_{\text{SiO}_2}^{\text{Opx}} & X_{\text{FeO}}^{\text{Opx}} & X_{\text{MgO}}^{\text{Opx}} & X_{\text{CaO}}^{\text{Opx}} \end{bmatrix} = \begin{bmatrix} 0 & 1 & 0 & 0 \\ 2 & 0.2 & 0.8 & 1 \\ 1 & 0 & 0 & 0 \\ -2 & 0.2 & 1.8 & 0 \end{bmatrix} \quad (\text{A6}).$$

Here we use the same mineral compositions of Eqn. A4, except that quartz ( $\text{SiO}_2$ ) substitutes for olivine. Of course, one need not take the transpose of the transformation matrix A6 if multiplication involves row matrices, and the order of the matrix multiplication is conducted as in Eqn. A3.1.

Finally, those PWDs that have large negative amounts of Opx when applying Eqns. A3-A4 can be described as positive combinations of garnet (Gar), Cpx, Periclase (Per), and Ol, using the equations:

$$\begin{bmatrix} F_{\text{Gar}} \\ F_{\text{Cpx}} \\ F_{\text{Per}} \\ F_{\text{Ol}} \end{bmatrix} = \begin{bmatrix} X_{\text{SiO}_2}^{\text{Gar}} & X_{\text{FeO}}^{\text{Gar}} & X_{\text{MgO}}^{\text{Gar}} & X_{\text{CaO}}^{\text{Gar}} \\ X_{\text{SiO}_2}^{\text{Cpx}} & X_{\text{FeO}}^{\text{Cpx}} & X_{\text{MgO}}^{\text{Cpx}} & X_{\text{CaO}}^{\text{Cpx}} \\ X_{\text{SiO}_2}^{\text{Per}} & X_{\text{FeO}}^{\text{Per}} & X_{\text{MgO}}^{\text{Per}} & X_{\text{CaO}}^{\text{Per}} \\ X_{\text{SiO}_2}^{\text{Ol}} & X_{\text{FeO}}^{\text{Ol}} & X_{\text{MgO}}^{\text{Ol}} & X_{\text{CaO}}^{\text{Ol}} \end{bmatrix}^{\text{T}-1} \times \begin{bmatrix} X_{\text{SiO}_2}^{\text{BSP}} \\ X_{\text{FeO}}^{\text{BSP}} \\ X_{\text{MgO}}^{\text{BSP}} \\ X_{\text{CaO}}^{\text{BSP}} \end{bmatrix} \quad (\text{A7})$$

and

$$\begin{bmatrix} X_{\text{SiO}_2}^{\text{Gar}} & X_{\text{FeO}}^{\text{Gar}} & X_{\text{MgO}}^{\text{Gar}} & X_{\text{CaO}}^{\text{Gar}} \\ X_{\text{SiO}_2}^{\text{Cpx}} & X_{\text{FeO}}^{\text{Cpx}} & X_{\text{MgO}}^{\text{Cpx}} & X_{\text{CaO}}^{\text{Cpx}} \\ X_{\text{SiO}_2}^{\text{Per}} & X_{\text{FeO}}^{\text{Per}} & X_{\text{MgO}}^{\text{Per}} & X_{\text{CaO}}^{\text{Per}} \\ X_{\text{SiO}_2}^{\text{Ol}} & X_{\text{FeO}}^{\text{Ol}} & X_{\text{MgO}}^{\text{Ol}} & X_{\text{CaO}}^{\text{Ol}} \end{bmatrix} = \begin{bmatrix} 4 & 0 & 4 & 0 \\ 2 & 0.2 & 0.8 & 1 \\ 0 & 0 & 1 & 0 \\ 1 & 0.2 & 1.8 & 0 \end{bmatrix} \quad (\text{A8})$$

where the mineral compositions of Ol and Cpx are as in Eqn. A4, but we now add the following mineral compositions: periclase (MgO) and pyrope garnet ( $\text{Mg}_4\text{Al}_3\text{Si}_4\text{O}_{12}$ ), the latter of which is compositionally indistinguishable from enstatite ( $\text{Mg}_2\text{Si}_2\text{O}_6$ ) or majorite garnet, both of which have the composition  $\text{Mg}_4\text{Si}_4\text{O}_{12}$  when expressed on the basis of 12 oxygens.

## Extended Data

Table A1. Polluted white dwarfs: compositions as weight % cations, and stellar properties.

| White Dwarf             | Source                           | Si   | Fe   | Mg   | Ca   | Disk? <sup>a</sup> | Atm <sup>b</sup> | SpT <sup>c</sup> | $T_{\text{eff}}(\text{K})^{\text{d}}$ | $\log(g)^{\text{e}}$ | $D(\text{pc})^{\text{f}}$ |
|-------------------------|----------------------------------|------|------|------|------|--------------------|------------------|------------------|---------------------------------------|----------------------|---------------------------|
| PG 0843+517             | Xu et al. (2019)                 | 7.9  | 87.9 | 4    | 0.2  | Y                  | H                | DAZ              | 24,670                                | 7.9                  | 136                       |
| WD 1929+011             | Melis et al. (2011)              | 16.3 | 57.8 | 25.1 | 0.8  | Y                  | H                | DAZ              | 23,470                                | 8.0                  | 53                        |
| WD 1536+520             | Farihi et al. (2016)             | 24.7 | 32.5 | 38.9 | 3.9  | Y                  | He               | DBAZ             | 20,800                                | 8.0                  | 205                       |
| PG 1015+161             | Xu et al. (2019)                 | 12.5 | 78.5 | 7.1  | 1.9  | Y                  | H                | DAZ              | 20,420                                | 8.1                  | 87                        |
| Ton 345                 | Jura et al. (2015)               | 32.1 | 44.2 | 21.6 | 2.2  | Y                  | He               | DBZ              | 18,700                                | 8.0                  | 107                       |
| WD 1041+092             | Melis and Dufour (2017)          | 32.6 | 9.8  | 46.8 | 10.9 | Y                  | He               | DBZ              | 18,330                                | 8.1                  | 174                       |
| HE 0106-3253            | Xu et al. (2019)                 | 7    | 84.6 | 4.9  | 3.5  | Y                  | H                | DAZ              | 17,350                                | 8.1                  | 69                        |
| GD 61                   | Farihi et al. (2013)             | 38.2 | 12.6 | 44.6 | 4.5  | Y                  | He               | DBAZ             | 17,280                                | 8.2                  | 54                        |
| G 241-6                 | Jura et al. (2012)               | 22   | 27.7 | 43.7 | 6.6  | N                  | He               | DBZ              | 15,300                                | 8.0                  | 73                        |
| GD 40                   | Jura et al. (2012)               | 20.6 | 38.2 | 31   | 10.2 | Y                  | He               | DBZ              | 15,300                                | 8.0                  | 64                        |
| WD 1551+175             | Xu et al. (2019)                 | 31.9 | 33.3 | 26.4 | 8.5  | Y                  | He               | DBZ              | 14,756                                | 8.0                  | 159                       |
| WD 2207+121             | Xu et al. (2019)                 | 29.8 | 37.4 | 29.6 | 3.2  | Y                  | He               | DBZ              | 14,752                                | 8.0                  | 166                       |
| WD 1145+017             | Fortin-Archambault et al. (2020) | 17.5 | 66.2 | 14.4 | 1.9  | Y                  | He               | DBAZ             | 14,500                                | 8.1                  | 142                       |
| WD 1425+540             | Xu et al. (2017)                 | 31.6 | 48.2 | 17.9 | 2.2  | N                  | He               | DBAZ             | 14,490                                | 8.0                  | 52                        |
| HS 2253+8023            | Klein et al. (2011)              | 19.8 | 49.5 | 25.3 | 5.4  | N                  | He               | DBZ              | 14,400                                | 8.4                  | 71                        |
| WD J0738+1835           | Dufour et al. (2012)             | 24.1 | 39.8 | 34.6 | 1.6  | Y                  | He               | DBZ              | 13,950                                | 8.4                  | 173                       |
| WD J1242+5226           | Raddi et al. (2015)              | 39.5 | 19.7 | 37.5 | 3.3  | N                  | He               | DBZ              | 13,000                                | 8.0                  | 161                       |
| G 29-38                 | Xu et al. (2014)                 | 36.6 | 36.5 | 21.4 | 5.5  | Y                  | H                | DAZ              | 11,820                                | 8.4                  | 18                        |
| WD 1232+563             | Xu et al. (2019)                 | 23.3 | 37.6 | 37.5 | 1.6  | ?                  | He               | DBZ              | 11,787                                | 8.3                  | 174                       |
| PG 1225-079             | Xu et al. (2013)                 | 23.5 | 50.1 | 18.1 | 8.2  | Y                  | He               | DZ               | 10,800                                | 8.0                  | 33                        |
| GD 362                  | Xu et al. (2013)                 | 19   | 58.4 | 11.9 | 10.8 | Y                  | He               | DBZ              | 10,540                                | 8.2                  | 56                        |
| Ross 640                | Koester and Wolff (2000)         | 33.8 | 10.7 | 52.1 | 3.4  | N                  | He               | DZ               | 8,500                                 | 8.0                  | 16                        |
| NLTT 43806              | Zuckerman et al. (2011)          | 34.8 | 17.4 | 37.9 | 9.9  | N                  | H                | DAZ              | 5,900                                 | 8.0                  | 71                        |
|                         | Lodders and Fegley (2018)        |      |      |      |      |                    |                  |                  | 5,780                                 |                      |                           |
| <i>Sun</i> <sup>g</sup> |                                  | 27.3 | 46.1 | 24.1 | 2.5  |                    |                  |                  |                                       | 4.4                  |                           |

(a) Indicates whether a disk of dust/gas has been detected. (b) The dominant element in the stellar atmosphere. (c) Stellar type: DA = H atmosphere; DB = He atmosphere; Z = polluted by "metals" (e.g., atomic number >2); DBAZ = both H and He lines are detected in the stellar atmosphere. (d)  $T_{\text{eff}}$  is the "effective temperature" which is a blackbody temperature that approximates the temperature of a star's photosphere. (e)  $\log$  of gravitational acceleration ( $\text{cm/s}^2$ ). (f) Distance from Sun (Brown et al. 2018). (g) Solar composition.



Table A2. Polluted white dwarfs as wt. % oxides, and Bulk Silicate Planet (BSP) compositions

|                         | Bulk Composition |                  |      |      | Bulk Silicate Planet <sup>a</sup> |                  |      |      | <i>Hollands et al.</i>   | <i>This Study</i>  |
|-------------------------|------------------|------------------|------|------|-----------------------------------|------------------|------|------|--|--|
|                         | SiO <sub>2</sub> | FeO <sub>t</sub> | MgO  | CaO  | SiO <sub>2</sub>                  | FeO <sub>t</sub> | MgO  | CaO  | ( <i>F<sub>cr</sub></i> )( <i>F<sub>m</sub></i> )( <i>F<sub>cst</sub></i> ) <sup>b</sup> | ( <i>F<sub>cr</sub></i> )( <i>F<sub>m</sub></i> )( <i>F<sub>cst</sub></i> ) <sup>c</sup> |
| PG 0843+517             | 12.3             | 82.6             | 4.9  | 0.2  | 58.7                              | 16.9             | 23.2 | 1.2  |  | (0.87)(0.13)(0)  |
| WD 1929+011             | 23.0             | 48.9             | 27.4 | 0.7  | 39.8                              | 11.4             | 47.5 | 1.2  |  | (0.41)(0.59)(0)  |
| WD 1536+520             | 32.1             | 25.4             | 39.2 | 3.3  | 40.3                              | 6.4              | 49.2 | 4.1  | (0.23)(0.77)(0)  | (0.17)(0.83)(0)  |
| PG 1015+161             | 18.8             | 71.0             | 8.3  | 1.8  | 55.0                              | 15.3             | 24.4 | 5.4  | (0.366)(0.325)(0.309)  | (0.79)(0.21)(0)  |
| Ton 345                 | 41.8             | 34.6             | 21.8 | 1.9  | 58.6                              | 8.3              | 30.5 | 2.6  |  | (0.32)(0.50)(0.18)   |
| WD 1041+092             | 39.8             | 7.2              | 44.3 | 8.7  | 42.1                              | 1.9              | 46.8 | 9.2  |  | (0)(1.0)(0)  |
| HE 0106-3253            | 10.9             | 79.5             | 6.0  | 3.6  | 44.1                              | 17.3             | 24.1 | 14.5 |  | (0.84)(0.16)(0)  |
| GD 61                   | 45.9             | 9.1              | 41.5 | 3.6  | 49.2                              | 2.4              | 44.6 | 3.8  | (0.032)(0.584)(0.384)  | (0.01)(0.99)(0)  |
| G 241-6                 | 28.7             | 21.6             | 44.1 | 5.6  | 34.6                              | 5.5              | 53.2 | 6.7  | (0.096)(0.384)(0.52)   | (0.13)(0.87)(0)  |
| G D40                   | 27.7             | 31.0             | 32.3 | 9.0  | 37.1                              | 7.7              | 43.2 | 12.0 | (0.098)(0.132)(0.77)   | (0.26)(0.74)(0)  |
| WD 1551+175             | 41.0             | 25.7             | 26.2 | 7.1  | 51.6                              | 6.4              | 33.0 | 9.0  |  | (0.23)(0.66)(0.11)   |
| WD 2207+121             | 38.5             | 29.1             | 29.7 | 2.7  | 50.4                              | 7.2              | 38.8 | 3.6  |  | (0.26)(0.74)(0)  |
| WD 1145+017             | 25.1             | 57.1             | 16.0 | 1.8  | 50.9                              | 12.9             | 32.6 | 3.7  | (0.457)(0.355)(0.188)  | (0.60)(0.40)(0)  |
| WD 1425+540             | 41.6             | 38.2             | 18.3 | 1.9  | 61.2                              | 9.0              | 26.9 | 2.8  |  | (0.36)(0.41)(0.23)   |
| HS 2253+8023            | 27.2             | 41.0             | 27.0 | 4.8  | 41.5                              | 9.8              | 41.2 | 7.4  | (0.299)(0.327)(0.374)  | (0.37)(0.63)(0)  |
| WD                      |                  |                  |      |      |                                   |                  |      |      |  |  |
| J0738+1835              | 31.7             | 31.6             | 35.3 | 1.4  | 42.8                              | 7.7              | 47.6 | 1.9  |  | (0.24)(0.76)(0)  |
| WD                      |                  |                  |      |      |                                   |                  |      |      |  |  |
| J1242+5226              | 47.8             | 14.4             | 35.2 | 2.6  | 53.8                              | 3.7              | 39.6 | 3.0  | (0.123)(0.57)(0.307)   | (0.07)(0.85)(0.08)   |
| G 29-38                 | 46.5             | 27.9             | 21.1 | 4.5  | 60.1                              | 6.8              | 27.2 | 5.9  | (0.175)(0.376)(0.448)  | (0.24)(0.48)(0.28)   |
| WD 1232+563             | 30.6             | 29.8             | 38.3 | 1.3  | 40.4                              | 7.4              | 50.5 | 1.8  |  | (0.21)(0.79)(0)  |
| PG 1225-079             | 32.2             | 41.2             | 19.2 | 7.4  | 49.3                              | 9.8              | 29.5 | 11.3 | (0.19)(0.047)(0.763)   | (0.44)(0.49)(0.07)   |
| GD 362                  | 27.0             | 49.9             | 13.1 | 10.0 | 47.5                              | 11.7             | 23.1 | 17.7 | (0.168)(0)(0.832)  | (0.57)(0.34)(0.09)   |
| Ross 640                | 40.8             | 7.7              | 48.7 | 2.7  | 43.4                              | 2.0              | 51.7 | 2.9  |  | (0)(1.0)(0)  |
| NLTT 43806              | 42.9             | 12.9             | 36.2 | 8.0  | 47.6                              | 3.3              | 40.2 | 8.9  | (0.042)(0.38)(0.579)   | (0.06)(0.94)(0)  |
| <i>Sun</i> <sup>d</sup> | 36.2             | 36.8             | 24.8 | 2.1  | 52.2                              | 8.9              | 35.8 | 3.1  |  | (0.35)(0.61)(0.04)   |

(a) Bulk silicate planet (BSP) compositions are calculated assuming that during core formation, Fe partitioning as on Earth, where  $\alpha_{Fe} = Fe^{m+cst}/Fe^{BP}$  ( $Fe^{m+cst}$  = total Fe in the mantle and crust;  $Fe^{BP}$  is Fe in the bulk planet, i.e., core + mantle crust) and  $\alpha_{Fe} = 0.27$  (see Putirka and Rarick 2019). (b) Fractions of crust ( $F_{cst}$ ), mantle ( $F_m$ ) and core ( $F_{cr}$ ) as calculated by Hollands et al. (2018), with renormalization so that their negative estimates become zero. (c) Fractions as in (b), as calculated in this study, using  $\alpha_{Fe} = 0.27$  and SiO<sub>2</sub>, MgO and FeO for mass balance and continental crust from Rudnick and Gao (2014) and a mantle composition from McDonough and Sun (1995), renormalized so that SiO<sub>2</sub> + FeO<sub>t</sub> + MgO + CaO = 100%. (d) Solar composition (Lodders and Fegley 2018).

Table A3. Possible matches of PWDs with Solar System Rock Types

| PWD           | Meteorite/Lunar Types From Bulk PWD <sup>a</sup> | Terrestrial Rock Types From Bulk PWD <sup>a</sup> | Rock Types From PWD BSP <sup>b</sup> | Mantle Mineralogy From PWD BSP <sup>c</sup> |
|---------------|--|---|--------------------------------------|---|
| PG 0843+517   | Iron   | -   | Shergottite                          | <b>Quartz Orthopyroxenite</b>               |
| WD 1929+011   | -  | -   | -                                    | Dunite                                      |
| WD 1536+520   | -  | -   | -                                    | <b>Pericase Dunite</b>                      |
| PG 1015+161   | Mesosiderite                                     | -   | Shergottite                          | <b>Quartz Pyroxenite</b>                    |
| Ton 345       | Shergottite                                      | -   | -                                    | <b>Quartz Orthopyroxenite</b>               |
| WD 1041+092   | -  | -   | -                                    | <b>Pericase Clinopyroxenite</b>             |
| HE 0106-3253  | Mesosiderite                                     | -   | Continental Picrite/Lunar Basalt     | Wehrlite                                    |
| GD 61         | Achondrite                                       | Continental Picrite                               | -                                    | Lherzolite                                  |
| G 241-6       | -  | -   | -                                    | <b>Pericase Wehrlite</b>                    |
| GD 40         | -  | -   | -                                    | <b>Pericase Wehrlite</b>                    |
| WD 1551+175   | Shergottite/Lunar Basalt                         | Continental Picrite                               | Continental Picrite                  | Lherzolite                                  |
| WD 2207+121   | Chondrite/Shergottite                            | -   | -                                    | Lherzolite                                  |
| WD 1145+017   | -  | -   | -                                    | Olivine Websterite                          |
| WD 1425+540   | Shergottite                                      | -   | -                                    | <b>Quartz Orthopyroxenite</b>               |
| HS 2253+8023  | -  | -   | -                                    | <b>Pericase Wehrlite</b>                    |
| WD J0738+1835 | -  | -   | -                                    | Dunite                                      |
| WD J1242+5226 | Shergottite                                      | Continental Picrite                               | -                                    | Harzburgite or Aubrite                      |
| G 29-38       | Shergottite/Lunar Basalt                         | -   | -                                    | <b>Quartz Pyroxenite</b>                    |
| WD 1232+563   | -  | -   | -                                    | <b>Pericase Dunite</b>                      |
| PG 1225-079   | -  | -   | Continental Picrite/Lunar Basalt     | Lherzolite                                  |
| GD 362        | -  | -   | Continental Picrite/Lunar Basalt     | Olivine Clinopyroxenite                     |
| Ross 640      | -  | -   | -                                    | <b>Pericase Dunite</b>                      |
| NLTT 43806    | Shergottite                                      | Continental Picrite                               | -                                    | Wehrlite                                    |
| <i>Sun</i>    | <i>Chondrite</i>                                 | -   | <i>Olivine Websterite</i>            | <i>Olivine Websterite</i>                   |

(a) Each rock type match is based on bulk PWD (polluted white dwarf) compositions (Fig. 1; Table A2) as compared to whole rock analyses of meteorites, Apollo mission samples and terrestrial rocks. (b) Rock type matches are as in (a), but for PWDs we use a "Bulk Silicate Planet" (BSP) composition, calculated by removing an Earth-like fraction of Fe to form a metallic core (Fig. 2; Table A2). (c) Mantle mineralogy calculated by mass balance using BSP compositions, and expressed as rock names using the ultramafic rock ternary of Le Bas and Streckeisen (1991; their Fig. 2; normal font in this table). All rock names in **bold italic** font are nominally exotic and, guided by Fig. 3, are named as follows: "quartz pyroxenites" have >10% each of orthopyroxene, clinopyroxene, and quartz; "quartz orthopyroxenites" have >10 % orthopyroxene and quartz, and < 10% clinopyroxene; "pericase dunites" have >10% each of pericase and olivine, and <10% clinopyroxene; "pericase wehrlites" contain >10% each of pericase, olivine and clinopyroxene; "pericase clinopyroxenites" have <10% olivine and >10% each of pericase and clinopyroxene.